Effects of the Protonation State of the EEEE Motif of a Bacterial Na^+-channel on Conduction and Pore Structure

Simone Furini,[†] Paolo Barbini,[†] and Carmen Domene[‡*]
[†]Department of Medical Biotechnologies, University of Siena, I-53100, Siena, Italy; and [‡]Chemistry Research Laboratory, University of Oxford, Oxford OX1 3TA, UK and Department of Chemistry, King's College London, London SE1 9NH

ABSTRACT A distinctive feature of prokaryotic Na^+-channels is the presence of four glutamate residues in their selectivity filter. In this study, how the structure of the selectivity filter, and the free-energy profile of permeating Na^+ ions are altered by the protonation state of Glu177 are analyzed. It was found that protonation of a single glutamate residue was enough to modify the conformation of the selectivity filter and its conduction properties. Molecular dynamics simulations revealed that Glu177 residues may adopt two conformations, with the side chain directed toward the extracellular entrance of the channel or the intracellular cavity. The likelihood of the inwardly directed arrangement increases when Glu177 residues are protonated. The presence of one glutamate residue with its chain directed toward the intracellular cavity increases the energy barrier for translocation of Na^+ ions. These higher-energy barriers preclude Na^+ ions to permeate the selectivity filter of prokaryotic Na^+-channels when one or more Glu177 residues are protonated.

INTRODUCTION

Structural-functional studies of eukaryotic Na^+-selective channels have greatly benefited from the availability of prokaryotic homologs that are expressed and characterized in heterologous systems (1), which has resulted in the elucidation of the crystallographic structures of three prokaryotic Na^+-channels: NaVAb (2), NaVRh (3), and NaVMS (4). When considering these structures to deduce general properties of Na^+-selective channels, the differences between eukaryotic and prokaryotic channels need to be contemplated. Prokaryotic channels are made of four identical protein chains that assemble to form a functional pore. Each of these four chains contributes with a glutamate residue to the selectivity filter (SF) of the channel, forming the so-called EEEE signature sequence. Instead, eukaryotic channels assemble from a single protein chain that includes four similar—but not identical—domains. These four domains contribute to the SF with different residues, namely aspartate, glutamate, lysine, and alanine. Thus, the EEEE signature sequence of prokaryotic Na^+-channels becomes DEKA in eukaryotes. Remarkably, if the DEKA sequence is mutated to the EEEE sequence, eukaryotic channels become selective to Ca^{2+} over Na^+ ions (5), whereas prokaryotic channels with the same signature sequence are selective to Na^+ over Ca^{2+} (2). The EEEE signature sequence might exhibit different protonation states in prokaryotic and eukaryotic channels because of the different local environment of the SF. Differences in the protonation states of these residues could be at least partially responsible for the difference in selectivity. Therefore, elucidating the effect that the number of protonated residues may have on the structure and conduction properties of prokaryotic Na^+-channels could provide a direct test for this hypothesis, and it may also offer insight into the functional role of charged residues in the SF. To this end, we have analyzed by molecular dynamics (MD) simulations and free-energy calculations, the structural and conduction properties of the NaVAb channel varying the protonation states of the EEEE signature sequence residues.

In the x-ray structure of NaVAb, the glutamate residues of the EEEE sequence (Glu177) have the side chain directed toward the extracellular entrance of the SF. Until now, most of the MD studies assumed the four Glu177 residues to be charged. In this scenario, the side chain oxygen atoms of Glu177 create an electronegative potential at the extracellular entrance of the SF. Not surprisingly, it was observed that Na^+ ions move from the extracellular solution to an empty SF in nanosecond equilibrium MD trajectories (6). Incoming ions first bind close to the side chains of the Glu177 residues; these are the residues that form the binding site S_{HFS}. Spontaneous translocations from S_{HFS} to a position at the intracellular entrance of the SF were also observed in a nanosecond timescale (6–8). At the intracellular side of the SF, the carbonyl oxygen atoms of residues Thr175 and Leu176 define two alternative binding sites for Na^+ ions. Since ions move fast between these two positions, we considered this extended region as if it were a single binding site (S_{CEN}). Potential of mean force (PMF) calculations with the umbrella sampling technique (9,10) confirmed the presence of binding sites S_{HFS} and S_{CEN}. According to the estimated PMFs, the energy barriers for Na^+ ions moving across the SF are low (<3 kcal/mol), and while an incoming ion assists the expulsion of an ion already inside the SF, ion movements are only loosely correlated. These conclusions were confirmed by metadynamics simulations, which proved the existence of several low-energy pathways for Na^+ ions across the SF of NaVAb

Submitted September 9, 2013, and accepted for publication April 3, 2014.
*Correspondence: carmen.domene@chem.ox.ac.uk
Editor: Bert de Groot
© 2014 by the Biophysical Society
0006-3495/14/05/2175/9 $2.00
http://dx.doi.org/10.1016/j.bpj.2014.04.005

(11). Finally, conduction in NaVAb and NaVMS has also been analyzed by nonequilibrium MD simulations with a constant electric field applied along the channel axis (11,12). Overall, the picture that emerged from nonequilibrium simulations is coherent with the description of ion conduction based on equilibrium PMF profiles. Inward conduction is a two-ion process that follows the same low-energy pathways obtained in metadynamics simulations (11). In the case of outward conduction, different occupancies of the SF were reported in NaVAb (11) and NaVMS (12), and the involvement of a third ion in the conduction process was also proposed. In these nonequilibrium MD simulations of ion conduction (11,12), as well as in the simulations used to estimate equilibrium PMFs reported in the literature (9–11), the structure of the SF did not depart from the crystallographic structure, and no major structural changes were observed for the side chains of Glu177.

An alternative conformation of Glu177 was observed in MD simulations with Ca^{2+} ions (8). As is the case with Na^+ ions, Ca^{2+} ions are attracted toward S_{HFS}. However, whereas the former make their way rapidly from S_{HFS} to S_{CEN}, the same transition is approximately ten times slower for Ca^{2+} ions. PMF profiles confirmed the presence of a higher-energy barrier for Ca^{2+} ions compared with Na^+ ions (~8 versus ~2 kcal/mol) between S_{CEN} and S_{HFS} (8,13). The larger hydration penalty paid by a Ca^{2+} ion in the middle of the SF may justify the higher-energy barrier experienced by this ion (13), but the structural changes of Glu177 may also play a role. Remarkably, the structural changes of Glu177 happen on a timescale of several nanoseconds, which could explain the variability between different PMF estimates (8,13). More recently, similar structural changes of the SF were described in extensive equilibrium MD simulations of NaVAb with Na^+ ions (14). The study by Chakrabarti et al. reported 47 equilibrium trajectories with a collated simulation time of 21.6 μs. States with two Na^+ ions in the SF were reported to be the most likely to occur (66%), followed by states with three (23%) and one ion (11%). In contrast with previous computational studies, this study observed that Glu177 residues can become highly mobile and switch between two conformations, with the side chain pointing toward the extracellular side of the channel, or directed to the pore lumen. Although further analyses are certainly needed to identify the role that the dynamics of Glu177 plays in the conduction process, increasing evidence suggests that a higher degree of flexibility of Glu177 might be a key factor for ion conduction (8,14).

Protonation of any of the Glu177 residues may modify the conduction mechanisms described so far by two nonexclusive mechanisms. First, protonation of Glu177 would reduce the negative charge at the extracellular entrance of the SF, which may have in turn an immediate electrostatic effect on the permeating ions. Second, protonation may alter the structure and the dynamics of the SF. Corry et al. analyzed the permeation properties of NaVAb in two situations: 1), with one protonated Glu177, and 2), with two protonated Glu177 in opposite subunits (9). It was reported that protonation of a single residue had a marginal effect on the free energy profile of a Na^+ or a K^+ ion moving along the SF. The affinity of the SF for cations was slightly reduced probably because of an increased electrostatic potential in the SF. Instead, the SF ceased to be attractive for cations when two Glu177 residues were protonated. S_{HFS} became energetically similar to the extracellular solution, and more surprisingly, S_{CEN} displayed an even higher energy. This effect is unlikely to be purely electrostatic. In this study, the behavior of the SF taking into account all the possible protonation states of the EEEE signature sequence has been analyzed. A nontrivial correlation between the protonation state, the structure of the SF, and the permeation properties has emerged.

METHODS

The atomic coordinates of the pore region of the NaVAb channel (residues 116 to 221) were defined as in the Protein Data Bank entry 3RVY (2). N- and C-terminals were amidated and acetylated respectively. This structure is in the closed conformation, and as reported for K^+-channels, it should be kept in mind when interpreting the computations (15). All the residues were modeled in their default protonation states at neutral pH with the exception of Glu177. Several combinations of protonation states were implemented for each of the four Glu177 residues: 1), all of them protonated, 2), all of them deprotonated, 3), one of them protonated, 4), three of them protonated, and 5–6) two of them protonated in opposite or adjacent protein subunits. The channel was inserted in a pre-equilibrated DOPC bilayer, with the channel axis aligned to the z axis of the simulation box and the aromatic belt defined by residues Trp95 aligned with the upper layer of the membrane. Water molecules (~20,000), Na^+ and Cl^- ions (up to a final concentration of 150 mM) were added using the tools implemented in visual molecular dynamics (VMD) (16). Harmonic restraints were initially applied to the backbone atoms of the protein and then gradually released. Umbrella sampling simulations were performed to examine the movement of one or two Na^+ ions across the SF (17). The reaction coordinate for the umbrella sampling simulations was the distance along the z axis between the restrained ion and the center of mass of the carbonyl oxygen atoms of Thr175 (Δz). Harmonic restraints with force constant of 10 kcal*mol*$Å^{-2}$ were applied to this reaction coordinate.

The sets of MD trajectories simulated for each PMF calculation are shown in Tables S1 to S4 in the Supplementary Material. The starting configurations for the umbrella sampling simulations of the one-ion permeation events were defined using the last snapshot of a 40 ns unrestrained MD trajectory. In contrast, the starting configurations for the simulations with two-ion permeation events were defined using the last snapshot of the one-ion umbrella sampling simulation with the ion inside the SF closer to one of the two restrained ions. In the event that a water molecule was closer than a restrained Na^+ ion to the center of the harmonic potential of a particular umbrella-sampling simulation, the positions of the water molecule and the ion were manually exchanged. Flat-bottom harmonic potentials were applied to keep the ions involved/not involved in the PMF calculations closer/further than 8.0 Å from the channel-axis. The value of the reaction coordinate was saved every 2 ps. Each simulation was initially conducted for 2 ns, and the cumulative average of the reaction coordinate in the last 1.95 ns was fitted by an exponential function. In the cases where the amplitude of the exponential function was higher than 0.1 Å for any of the restrained ions, the trajectory of the window was extended by 0.5/0.1 ns

respectively for the one- and two-ion simulations. This last step was repeated until the amplitude of the exponential function decreased below 0.1 Å. The purpose of this protocol is to remove any possible nonstationary phase from the umbrella sampling trajectories in a systematic way.

Nonstationary phases appeared in some trajectories as a consequence of structural changes in the SF. The threshold value used for the amplitude of the fitting exponential function is obviously arbitrary, and it was based on visual inspection of the critical trajectories (see an example in Fig. S10 in the Supplementary Material). A threshold value of 0.05 Å gave analogous results in terms of energy profiles on a test case. At each iteration, the cumulative average was calculated considering only the final 2 ns, with the last 1.95 ns used for the exponential fitting. Once the protocol converged for all the umbrella sampling windows, the PMF was calculated by the WHAM algorithm using the final 2 ns of each trajectory. The same fragment of the umbrella sampling trajectories was used for the structural analyses. Average values and standard deviation of the one-dimensional PMF were estimated dividing each trajectory into three sections, and calculating the PMF separately for each data set. The same procedure was used to analyze each combination of protonation states for the EEEE signature sequence.

For each protonation state, electrical neutrality was maintained by removing Na^+ ions from the bulk solution. The total simulation time in this study was ~1.6 μs; a breakdown per system is reported in the Supplementary Material. MD trajectories were simulated using NAMD version 2.9 (18), with the CHARMM27 force field with CMAP corrections (19), and the TIP3P model for water molecules (20). Simulations were performed in the NpT ensemble. Pressure was kept at 1 atm by the Nose-Hoover Langevin piston method (21,22), with a damping time constant of 100 ps and a period of 200 ps. Temperature was kept at 300 K by coupling the system to a Langevin thermostat, with a damping coefficient of 5 ps^{-1} (22). Electrostatics interactions were treated by the Particle Mesh Ewald algorithm, with grid spacing below 1 Å (23). Van der Waals interactions were truncated at 12 Å, and smoothed at 10 Å. Hydrogen atoms were restrained by the SETTLE algorithm (24), which allowed a 2 fs time-step.

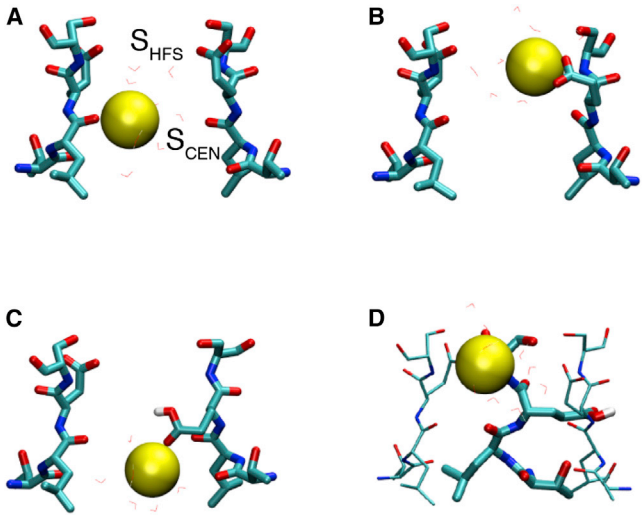

FIGURE 1 Panels illustrate the structures of the selectivity filter of NaVAb. Sodium ions are represented as yellow spheres, and water molecules within 3.5 Å of the ion are shown in red, in line representation. Panels (A) and (B) show two opposite subunits of the SF in licorice, when four Glu177 residues are charged. Panel (A) shows a conformation of the SF similar to the crystallographic structure. Binding sites S_{HFS} and S_{CEN} are highlighted. In panel (B), the χ2 dihedral angle of Glu177 in the right subunit is changed to ~50°. Panels (C) and (D) show structures of the SF with one Glu177 residue protonated. Panel (C) shows two opposite subunits for a conformation with the side chain of the protonated glutamate directed toward S_{CEN}. Panel (D) shows two opposite subunits (with Glu177 in the charged state) in thin lines, with a third subunit (with Glu177 protonated) in thick line. The side chain of the protonated Glu177 residue lies at the back of the SF. To see this figure in color, go online.

RESULTS

Six different combinations of protonation states for each of the four glutamate residues (Glu177) in the SF of NaVAb are theoretically possible: all the residues negatively charged; one, three, or four protonated Glu177 residues; and two protonated Glu177 residues either in opposite or adjacent subunits. We first describe the behavior of the SF with four charged Glu177 residues. In this situation, the crystallographic structure of the SF (Fig. 1 *A*) is stable in MD simulations in the nanosecond timescale (6,9,10). In this study, several MD trajectories were simulated with a Na^+ ion restrained at different positions along the channel-axis, spanning the region from the intracellular cavity to the extracellular compartment. The overall structure of the SF is largely unaffected by the location of the permeating ion, as evidenced by the orientation of Glu177 (Fig. 2 *A*) and the distances between atoms of the SF (Fig. S1) as a function of ion position. The side chains of Glu177 residues are always directed toward the extracellular side of the channel (Fig. 2 *A*). This particular orientation is stabilized by interactions with residues Gln172 and Ser178 of the same subunit, and residues Ser178 and Ser180 of the adjacent subunit (Fig. S1). All the distances between these sets of atoms are conserved, regardless of the position of the permeating Na^+ ion. The interaction between the side chain oxygen atom of Thr175 and the side chain nitrogen atom of Trp179 of the adjacent subunit (Fig. S1) is also maintained, contributing to the stability of binding site S_{CNS}.

The PMF of a single Na^+ ion moving along the SF when four charged glutamates are considered (Fig. 3 *A*) was similar to the ones reported previously (6,9,10). The free energy of an ion occupying S_{HFS} is -7.5 kcal/mol lower than when the ion is in the extracellular solution, and the energy is -4.8 kcal/mol lower in S_{CEN}, than in the intracellular cavity (Table 1). This PMF profile preserves all the main features reported in a previous PMF calculated using MD trajectories of 0.5 ns (10), with the exception of an increase of ~1 kcal/mol when the ion occupies S_{HFS}. This difference with our previous computations could be attributed to a deficient sampling of the configurational space of the Glu177 residues when the ion is close to S_{HFS}. In the current simulation protocol, the umbrella sampling trajectories are extended until no drift is observed for the *z*-coordinate of the ion (see the Methods section). The trajectory that required the longest time to reach an equilibrated state was the one with the ion restrained at the intracellular side of S_{HFS} ($\Delta z = 6$ Å, where Δz is equal to the distance along the channel-axis between the Na^+ ion and the center of the carbonyl oxygen atoms of Thr175). This trajectory is also

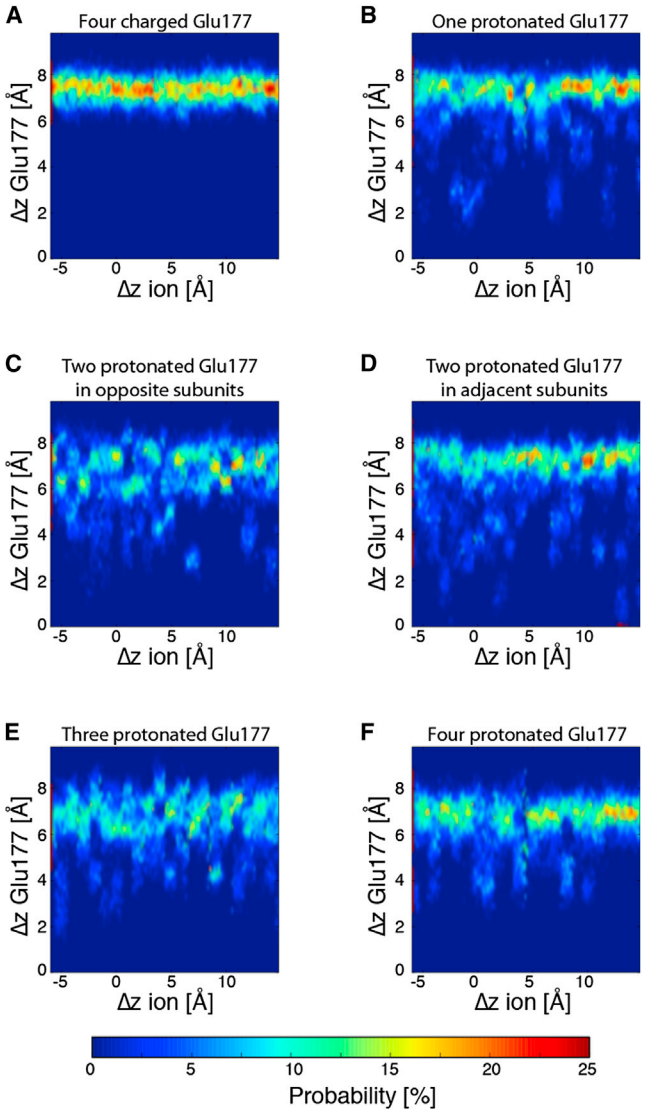

FIGURE 2 Probability histograms are shown for the position of the side chain of Glu177 residues as a function of the position of the permeating ion in a SF with (A) four charged glutamates; (B) one protonated glutamate; (C) two protonated glutamates in opposite side chains; (D) two protonated glutamates in adjacent side chains; (E) three protonated glutamates; and (F) four protonated glutamates. Values on the *x* and *y* axis (Δz ion/Δz Glu177, respectively) correspond to the distance along the channel axis between the center of mass of the carbonyl oxygen atoms of residue Thr175 and the permeating ion (*x* axis) or the center of mass of the side chain oxygen atoms of one Glu177 residue (*y* axis). Probability histograms were produced by discretizing the *x* and *y* axis in bins with size 0.2 Å. Histograms corresponding to the position of the four Glu177 residues were added, and then normalization was applied along each *x*-coordinate. To see this figure in color, go online.

the only one where conformations of the Glu177 residues with the side chain directed toward the pore lumen were observed (Fig. 1 *B*). Conformations of Glu177 pointing to the pore lumen are characterized by positive values of the dihedral angle χ_2 (C_α-C_β-C_γ-C_δ), whereas negative values characterize the outward orientation of Glu177. In the MD trajectory with the permeating ions restrained below S_{HFS} ($\Delta z = 6$ Å), the probability of positive χ_2 values is 62%. This trajectory required 9 ns to reach equilibrium, which is in agreement with the relaxation time estimated for structural transitions of the Glu177 residues in microseconds MD trajectories (14).

The structure of the SF changed significantly when one Glu177 residue was protonated. In contrast to what was observed with four charged glutamates, the side chain of the protonated Glu177 is not always directed toward the extracellular side of the channel (Fig. 2 *B*). Instead, conformations with this side chain pointing to S_{CEN} (Fig. 1 *C*), or lying at the back of the SF (Fig. 1 *D*) were also observed. These conformations of Glu177 differ from the ones described previously. In the former case, when four glutamates are charged, the two conformations of Glu177 (side chain in the outward direction or pointing to the pore lumen) differ in the value of the dihedral angle χ_2, whereas χ_1 (N-C_α-C_β-C_γ) is conserved. This was also reported in microsecond simulations (14). In contrast, the novel conformations of the protonated glutamate are characterized by a 90° rotation of χ_1. The protonation of a single glutamate residue seemed to confer higher flexibility not only to the residue per se but to the entire SF. When four or three charged glutamate residues are involved, the root mean square deviation of the backbone atoms of residues Thr175 to Ser180 with respect to the x-ray structure is 0.52 ± 0.06 Å and 0.76 ± 0.20 Å, respectively. Moreover, the structure of the SF became sensitive to the position of the permeating ion. When the ion is at the intracellular side of binding sites S_{CEN} ($\Delta z = -1$Å) or S_{HFS} ($\Delta z = 6$Å), the hydrogen bond between Thr175 and Trp179 is broken in all the subunits, while an interaction between Trp179 and the side chain of the protonated glutamate is formed (Figs. S2 and S3). Not surprisingly, this alternative structure of the SF exhibited a distinctive energy profile for a permeating Na^+ ion (Fig. 3 *B*). Both binding sites, S_{HFS} and S_{CEN}, are much less attractive to Na^+ ions than in the case with four charged glutamates: 2.9 kcal/mol versus -7.5 kcal/mol for an ion coming from the extracellular solution, and -2.0 kcal/mol versus -4.8 kcal/mol for an ion coming from the channel cavity. Furthermore, S_{HFS} is 8.2 kcal/mol higher in energy than S_{CEN}, compared with a value of 1.6 kcal/mol with four charged glutamates (Table 1). The structural changes of the SF are a major determinant of these energetic differences. Indeed, a PMF profile calculated using only the first nanosecond of each umbrella sampling trajectory—when most of these changes have not taken place yet—showed a much smaller difference in energy between S_{CEN} and S_{HFS} (dotted line in Fig. 3 *B*).

A comparison between the one-dimensional energy profiles in the presence of four or three charged glutamates in the SF reveals that when one glutamate is protonated, the binding site S_{HFS} is highly destabilized with respect to S_{CEN}. With four charged glutamates, the SF has two binding

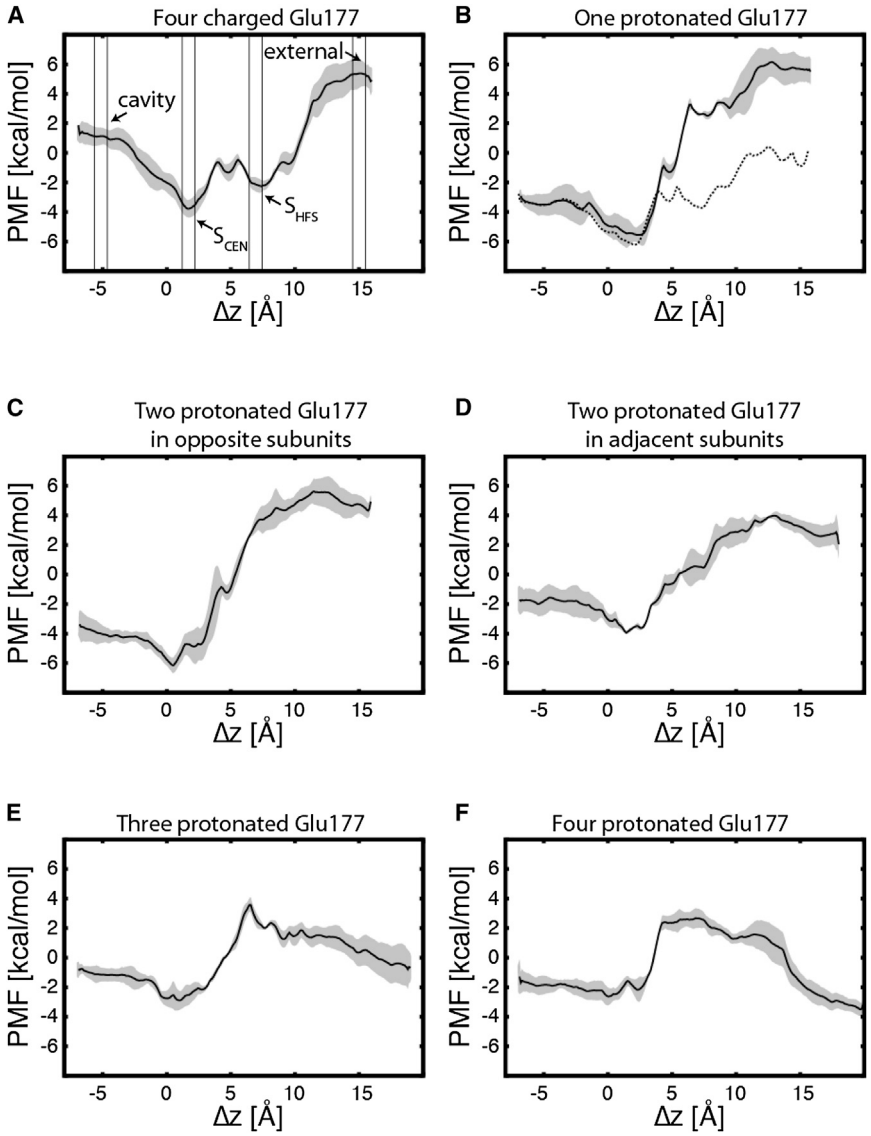

FIGURE 3 Panels illustrate the potential of mean force (PMF) for the translocation of a Na^+ ion along the SF of NaVAb. Δz is the distance along the channel axis between the permeating ion and the center of mass of the carbonyl oxygen atoms of residues Thr175. The average PMF is shown as a continuous black line for a SF with (A) four charged Glu177 residues; (B) one protonated Glu177 residue; (C) two protonated Glu177 residues in opposite side chains; (D) two protonated Glu177 residues in adjacent side chains; (E) three protonated Glu177 residues; and (F) four protonated Glu177 residues. The gray shaded region corresponds to ± one standard deviation. The vertical lines in panel (A) delimit the regions used to define the energy values of an ion in the cavity, S_{CEN}, S_{HFS}, and in the extracellular compartment reported in Table 1. In panel (B) a dotted line is used to show the PMF calculated with 1-ns window trajectories.

sites with similar energies separated by a low-energy barrier. Thus, an ion can easily switch between these two positions. The energetic balance between S_{CEN} and S_{HFS} is crucial for efficient ion conduction across the SF. However, with one protonated glutamate, the binding sites are energetically unbalanced, and this could impede ion conduction. To test this hypothesis, we calculated the PMF in the presence of two ions. The same protocol employed for the one-dimensional simulations was used to test the convergence of the umbrella sampling trajectories. In the case of four charged glutamates, the energy map was analogous to the one previously calculated with 0.5 ns trajectories (10), with the exception of a slightly higher energy when the lowermost ion was in S_{HFS} in agreement to what was observed in the one-dimensional PMF (Fig. 4 *A*). With four charged glutamates, the lowest energy configuration has two ions in the SF, in S_{CEN} and S_{HFS}, respectively. Configurations with one ion in the SF at binding site S_{HFS}, and the second ion inside or outside the channel are ~3 kcal/mol higher in energy. To get a semi-quantitative estimate of the channel conductance, we performed random-walk simulations of ions in the SF, with the transition rates determined from the PMF profiles. This approach is similar to the one adopted by Bernèche and Roux in early work with the KcsA potassium channel (25). Details about the procedure are provided in the Supplementary Material.

The random-walk simulations gave an estimate of channel conductance of ~100 pS (Fig. S9), which is around three times higher than the experimental value (12). Considering the numerous simplifications adopted in the random-walk simulations (e.g., only the resistance of the SF is considered; the transmembrane potential is modeled as a constant electric field across the SF; a constant diffusion coefficient is assumed for Na^+ ions), and the inherent difficulties of free-energy calculations, this slight difference with the experimental data is noteworthy. As expected from the

TABLE 1 Binding sites S_{CNS} and S_{HFS}

Number of protonated residues	$\langle G_{CEN}\rangle - \langle G_{CAV}\rangle$ [kcal/mol]	$\langle G_{HFS}\rangle - \langle G_{EXT}\rangle$ [kcal/mol]	$\langle G_{HFS}\rangle - \langle G_{CEN}\rangle$ [kcal/mol]
0	-4.8	-7.5	+1.5
1	-2.0	-2.9	+8.2
2 opposite subunits	-0.8	-1.3	+8.2
2 adjacent subunits	-1.9	-2.7	+4.2
3	-1.3	+2.2	+5.1
4	0.0	+4.3	+4.4

Binding energy for S_{CEN} site is defined as the difference between $\langle G_{CEN}\rangle$ and $\langle G_{CAV}\rangle$, where $\langle G_{CEN}\rangle$ is the average energy in the range 1.3 Å$<\Delta z<$2.3 Å, and $\langle G_{CAV}\rangle$ is the average energy in the range -5.5 Å$<\Delta z<$-4.5 Å. Δz is defined as the distance from the center of mass of the carbonyl oxygen atoms of residue Thr175 along the channel-axis. The binding energy for site S_{HFS} is defined as the difference between $\langle G_{HFS}\rangle$ (average energy in the range 6.5 Å$<\Delta z<$7.5 Å) and $\langle G_{EXT}\rangle$ (average energy in the range 14.5 Å$<\Delta z<$15.5 Å).

one-dimensional energy profiles, also the two-dimensional (2D) PMF changed abruptly when one protonated glutamate was considered (Fig. 4 *B*). In this case, the most stable configuration has only one ion inside the SF at binding site S_{HFS}, with the second ion at the extracellular side of the channel. A similar configuration with the second ion at the intracellular side of the channel can be envisaged, although it was not observed in the present study because the intracellular gate is closed. Moving the second ion closer to the SF has an energetic cost of ~3 kcal/mol, and a further energetic cost of ~2 kcal/mol is associated with the inward movement of the ion in the SF from S_{HFS} to the intracellular cavity. The same structural changes described with one ion in the SF were observed in the presence of two permeating ions. The conductance estimated from the random-walk simulations with one protonated glutamate was more than ten times lower (0.05-folds at 25 mV) than the value obtained with four charged glutamates in the SF (Fig. S9). Because of the exponential dependence between the free energy and the transition rates in the SF, care must be taken when interpreting the results in terms of channel conductance. The energy barriers for conduction events in a SF with a protonated glutamate are ~1 kcal/mol higher than the barriers when four charged glutamates are considered. To validate the differences in conductance, we performed a block-analysis. The last 2 ns of each umbrella-sampling trajectory were divided into three parts, and the free energy profile was calculated for each data set, obtaining three independent energy maps for each protonation state. The average value and the standard deviation of the currents were calculated performing random-walk simulations with these three energy profiles. The difference in current between the channel with four charged glutamates or one protonated glutamate was much higher than the estimated standard deviations (Fig. S9), suggesting that sampling errors do not alter the conclusions about channel conductance. Inaccuracies because of inefficient sampling are obviously not the only source of errors in free energy calculations; approximations inherited in the adopted force field are potentially another shortcoming (26). However, we can safely conclude that protonation of a single glutamate residue, and the associated structural changes of the SF, have a considerable impact on the free energy profile experienced by permeating ions, which it is likely to result in a decrease in channel conductance.

Protonation of two glutamates on opposite subunits gave a one-dimension PMF similar to the one obtained with only one protonated glutamate (Fig. 3 *C*). The binding energies of a Na^+ ion at S_{HFS} or S_{CEN} further decreased by ~1 kcal/mol, and the difference in energy between the two binding sites remained the same (Table 1). In contrast, a remarkable change in the PMF profile was observed in the presence of two protonated glutamate residues in adjacent subunits (Fig. 3 *D*). In this conformation, the difference in energy between S_{CEN} and S_{HFS} was 4.2 kcal/mol, compared with 8.2 kcal/mol in the previous case (Table 1). The energetic differences between a channel with protonated

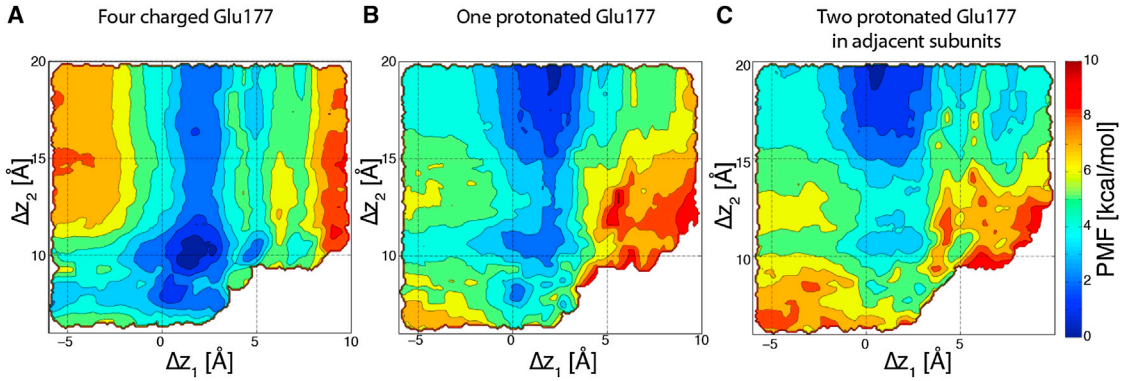

FIGURE 4 Panels show the potential of mean force (PMF) for the translocation of two Na^+ ions: (A) SF with four charged Glu177 residues, (B) SF with one protonated Glu177 residue, and (C) SF with two protonated glutamates in opposite subunits. $\Delta z_{1/2}$ are the distances along the channel axis between the permeating ions and the center of mass of the carbonyl oxygen atoms of residues Thr175. Contour lines are drawn every 1 kcal/mol. To see this figure in color, go online.

glutamate residues in opposite or adjacent subunits can easily be explained when considering the structure of the SF (Fig. 2 *C* and *D* and Figs. S4 and S5). If the analysis is limited to the samples with a Na^+ ion between S_{CEN} and S_{HFS}—where the highest difference in energy is observed—the side chains of the two protonated glutamate residues are situated below the carbonyl carbon of Glu177 with a probability of 63% in the case of protonated residues on opposite side chains. This probability is similar to the one observed with only one protonated Glu177 (51%). In contrast, the probability of observing a protonated Glu177 residue in the inwardly oriented conformation decreases to 15% in the case of protonated residues on adjacent subunits. Thus, for protonated glutamates on opposite subunits the side chain of a Glu177 occupies the permeation pathway most of the time, while this is not the case when the protonated glutamates are next to each other (Fig. S8). Since the characteristics of the channel with two protonated glutamates in adjacent side chains resembled the channel with four charged glutamates (e.g., energy difference between S_{HFS} and S_{CEN}, and lower probability for the inwardly directed configuration of Glu177 compared with the channel with one protonated glutamate or two protonated glutamates on opposite subunits), the 2D energy profile for this protonation state was computed (Fig. 4 *C*). The shape and the energy barriers of the 2D energy profile as well as the estimated channel conductance (Fig. S9) are remarkably similar to those obtained when only one protonated glutamate is considered. A significant difference is the reappearance of a local energy minimum with two ions close to S_{HFS} ($\Delta z_1 = 5$ Å and $\Delta z_2 = 10$ Å). This may be related to the lower probability of the inwardly directed configuration of Glu177 in this protonation state of the SF. The high similarity between the 2D energy maps with one or two protonated glutamates suggests that the same event—reorientation of Glu177 residues—is likely responsible for the changes in free energy in both the scenarios.

The remaining combinations of protonation states of the SF were analyzed considering only one-dimensional permeation events. This can be justified considering that with one/two protonated glutamate the most likely configuration has only one ion in the SF, and it is unlikely that more ions occupy a SF with less negatively charged residues. The possibility of observing a protonated Glu177 residue in the inward conformation is low when three or four Glu177 residues are protonated (Fig. 2 *E* and *F*). Limiting the analyses to the umbrella sampling trajectories with a Na^+ ion between S_{CEN} and S_{HFS}, the inward conformation of a protonated Glu177 residue is observed with probabilities of 31% and 25%, respectively, in the presence of three or four protonated glutamates. Like in the case of two protonated Glu177 residues in adjacent subunits, these protonation states are characterized by an energy difference of 4 to 5 kcal/mol between S_{CNS} and S_{HFS}. However, it should be noted that in these situations, the binding site S_{HFS} ceases to attract Na^+ ions (energy value higher than at the extracellular compartment), whereas S_{CEN} slightly attracts an ion coming from the intracellular cavity only when three, and not four, Glu177 residues are protonated (Table 1 and Fig. 3 *E* and *F*). Conformations with the side chain of Glu177 pointing inward were never observed for charged residues for all the possible combinations of protonation states of the EEEE sequence.

DISCUSSION

How the SF of NaVAb behaves when some of the Glu177 residues are protonated is an intriguing case study for several reasons. First, these four glutamates in the SF are confined in a limited region. Thus, it is possible that some of them are indeed protonated at physiological conditions. Besides, the EEEE signature sequence is responsible for selectivity to Na^+ in prokaryotic channels, and Ca^{2+} in eukaryotic channels. Therefore, a different protonation state of these glutamate residues might be partially responsible for the different selectivity observed. Finally, eukaryotic Na^+-channels are characterized by the DEKA signature sequence, instead of the EEEE sequence of bacterial Na^+-channels. As a result, analyzing different protonation states of NaVAb might provide indirect clues about the functioning of eukaryotic channels. The work presented in this study shows that protonation of a single glutamate residue is enough to radically modify the PMF experienced by a Na^+ ion that moves across the SF. In the presence of a single protonated glutamate, binding sites S_{CEN} and S_{HFS} become less appealing for an incoming Na^+ ion, as expected from the reduction in the electrostatic attraction, and more surprisingly, a high-energy difference emerges between sites S_{CEN} and S_{HFS}. This result disagrees with a previous study (9) where similar energy profiles were reported for four or three charged glutamate residues. Although there are several differences between the simulation protocols employed in both studies (i.e., the definition of the reaction coordinate and the ion parameters), it is hard to believe that these differences alone explain these discrepancies. It might be that the structural changes of the SF that were sampled in the current study in the case of a system with just one protonated glutamate residue are responsible for the contrasting PMF profiles. In agreement with this hypothesis, the PMF profile calculated with 1-ns trajectories—when most of the structural changes of the SF have yet to take place—was similar to the one calculated with four charged glutamate residues. Because of the long relaxation times associated with the structural changes of Glu177, the length of the simulations is certainly more critical in the studies of this system in comparison with similar studies on K^+-channels (27).

Relaxation times in the nanosecond timescale were reported also in simulations with four charged glutamates, which switched between conformations with the side chain

oriented away or toward the pore lumen. These two conformations resemble the ones recently described by Chakrabarti et al. (14). Indeed, the two alternative conformations of Glu177 sampled by Chakrabarti et al. differ mainly in the χ_2 dihedral angle of Glu177 (C_α-C_β-C_γ-C_δ), with sets of conformations characterized by negative (side chain of Glu177 directed outward), or positive (side chain of Glu177 directed to the pore lumen) χ_2 values, whereas χ_1 remained almost unchanged in both situations. In other words, the carboxyl oxygen atoms of charged glutamates may point to the extracellular solution or to the pore lumen, but unlikely to the intracellular solution. Switching between these two conformations of Glu177 has only a marginal effect on the PMF of a permeating Na^+ ion, i.e., a slightly increase in the binding energy of S_{HFS}. In contrast, the structural changes sampled when any or all glutamates are protonated had a severe impact on the PMF of permeating ions. In addition to the conformations observed with charged glutamates, protonated glutamates exhibited a third conformation, with the carboxyl oxygen atoms pointing to S_{CEN}. The likelihood of this conformation correlates with the energy difference between S_{CEN} and S_{HFS}. When glutamate residues on opposite subunits are protonated, the probability to have at least one glutamate residue pointing to S_{CEN} is high, and so the difference in energy between S_{CEN} and S_{HFS}. This probability decreases when two protonated residues are in adjacent subunits, or three and four residues are protonated, and in these situations, the energy difference between S_{CEN} and S_{HFS} decreases as well.

The atomic model used in the MD simulations has the intracellular gate closed. Thus, it is not possible to simulate complete conduction events, and therefore to make a direct link between the data presented in this study and the conduction properties of the channel. However, the free-energy maps show that in the presence of a protonated glutamate, binding sites S_{CEN} and S_{HFS} are energetically unbalanced, and this likely hampers ion conduction. A semi-quantitative estimate of the channel conductance obtained by random-walk simulations, seemed to confirm this hypothesis. Protonation of a single glutamate residue reduced the channel conductance by an order of magnitude. According to these data, the conductive state of prokaryotic Na^+ channels requires four charged glutamates in the SF. Thus, it is unlikely that different protonation states of the EEEE signature sequence could be responsible for the different selectivity of prokaryotic and eukaryotic channels with the same EEEE signature. The presence of other acidic residues in the surrounding of the SF is likely to have key implications (28).

The MD simulations presented in this study reveled a strong correlation between the energetic unbalance of S_{HFS} and S_{CEN} and the likelihood of the inwardly directed configuration of residues Glu177, which may play a role in the exclusion of Ca^{2+} ions from permeation events in NaVAb. Indeed, in the case of Ca^{2+} ions, conformations of Glu177 with the side chain inwardly oriented were already observed (8), and likewise, an energy difference between S_{CEN} and S_{HFS} emerged. The residues surrounding the EEEE signature sequence might exert some control on the conformations accessible by this motif, which could explain why the same EEEE signature sequence exhibits contrasting selectivity in different channels. Further work is required to test this hypothesis.

Another study that investigates the role of the protonation of Glu177 residues in NaVAb by MD simulations was published during the review process of this manuscript (29). The results presented are similar when two or more protonated glutamates are considered, whereas different conclusions were reached in the case of one protonated glutamate. Boiteux et al. estimated the free energy from an unbiased MD trajectory of 2.5 μs, whereas we use biased trajectories with a cumulative simulated time of ~0.4 μs (29). The harmonic biases guarantee a more efficient sampling of the configurational space, thus higher accuracy of the free-energy estimates at the same computational cost. However, in each umbrella sampling simulation of the length described here, the SF can rearrange itself around the ions but it cannot switch to a different metastable state, whereas in a single microsecond-long trajectory, transitions between different states of the SF are possible. In the simulation by Boiteux et al., the structure of the SF evolved during the trajectory, with a structural change that was suggested to be associated to channel inactivation, and that began after 0.25 μs. In microsecond simulations of ion conduction in K^+ channels, it was necessary to modify the parameters of the force field to avoid the evolution of the system toward an unnatural state (30). Similar processes could arise in simulations of Na^+ channels, and therefore, computational techniques such as umbrella sampling—where many trajectories are used starting from the same equilibrated structure—might be preferred to approaches based on a single microsecond trajectory. In contrast, if structural changes in the microsecond timescale are part or a result of the conduction events, each umbrella sampling trajectory need to be long enough to sample these transitions, which would represent a severe shortcoming for this computational strategy.

SUPPORTING MATERIAL

Four tables and ten figures are available at http://www.biophysj.org/biophysj/supplemental/S0006-3495(14)00386-5.

This work was supported by CINECA Award N. HP10BX4MV5, 2013. C. Domene would like to acknowledge the use of computational resources from the EPSRC UK National Service for Computational Chemistry Software (NSCCS) and the Hartree Center.

REFERENCES

1. Charalambous, K., and B. A. Wallace. 2011. NaChBac: the long lost sodium channel ancestor. *Biochemistry.* 50:6742–6752.

2. Payandeh, J., T. Scheuer, …, W. A. Catterall. 2011. The crystal structure of a voltage-gated sodium channel. *Nature.* 475:353–358.
3. Zhang, X., W. Ren, …, N. Yan. 2012. Crystal structure of an orthologue of the NaChBac voltage-gated sodium channel. *Nature.* 486:130–134.
4. McCusker, E. C., C. Bagneris, …, B. A. Wallace. 2012. Structure of a bacterial voltage-gated sodium channel pore reveals mechanisms of opening and closing. *Nature Comm.* 3:1102. http://dx.doi.org/10.1038/ncomms2077.
5. Heinemann, S. H., H. Terlau, …, S. Numa. 1992. Calcium channel characteristics conferred on the sodium channel by single mutations. *Nature.* 356:441–443.
6. Carnevale, V., W. Treptow, and M. L. Klein. 2011. Sodium ion binding sites and hydration in the lumen of a bacterial ion channel from molecular dynamics simulations. *J. Phys. Chem. Lett.* 2:2504–2508.
7. Qiu, H., R. Shen, and W. Guo. 2012. Ion solvation and structural stability in a sodium channel investigated by molecular dynamics calculations. *Biochim. Biophys. Acta.* 1818:2529–2535.
8. Ke, S., E. M. Zangerl, and A. Stary-Weinzinger. 2013. Distinct interactions of Na^+ and Ca^{2+} ions with the selectivity filter of the bacterial sodium channel Na(V)Ab. *Biochem. Biophys. Res. Commun.* 430:1272–1276.
9. Corry, B., and M. Thomas. 2012. Mechanism of ion permeation and selectivity in a voltage gated sodium channel. *J. Am. Chem. Soc.* 134:1840–1846.
10. Furini, S., and C. Domene. 2012. On conduction in a bacterial sodium channel. *PLOS Comput. Biol.* 8:e1002476.
11. Stock, L., L. Delemotte, …, M. L. Klein. 2013. Conduction in a biological sodium selective channel. *J. Phys. Chem. B.* 117:3782–3789.
12. Ulmschneider, M. B., C. Bagnéris, …, B. A. Wallace. 2013. Molecular dynamics of ion transport through the open conformation of a bacterial voltage-gated sodium channel. *Proc. Natl. Acad. Sci. USA.* 110:6364–6369.
13. Corry, B. 2013. Na^+/Ca^{2+} selectivity in the bacterial voltage-gated sodium channel NavAb. *PeerJ.* 1:e16.
14. Chakrabarti, N., C. Ing, …, R. Pomès. 2013. Catalysis of Na^+ permeation in the bacterial sodium channel Na(V)Ab. *Proc. Natl. Acad. Sci. USA.* 110:11331–11336.
15. Domene, C., S. Vemparala, …, M. L. Klein. 2008. The role of conformation in ion permeation in a K^+ channel. *J. Am. Chem. Soc.* 130:3389–3398.
16. Humphrey, W., A. Dalke, and K. Schulten. 1996. VMD: visual molecular dynamics. *J. Mol. Graph.* 14:33–38.
17. Domene, C., S. Furini, …, M. H. Jo. 2009. Examining Ion Channel Properties Using Free-Energy Methods. *In* Methods in Enzymology Academic Press, New York, pp. 155–177.
18. Phillips, J. C., R. Braun, …, K. Schulten. 2005. Scalable molecular dynamics with NAMD. *J. Comput. Chem.* 26:1781–1802.
19. MacKerell, A. D., D. Bashford, …, M. Karplus. 1998. All-atom empirical potential for molecular modeling and dynamics studies of proteins. *J. Phys. Chem. B.* 102:3586–3616.
20. Jorgensen, W. L., J. Chandrasekhar, …, M. L. Klein. 1983. Comparison of simple potential functions for simulating liquid water. *J. Chem. Phys.* 79:926–935.
21. Martyna, G. J., D. J. Tobias, and M. L. Klein. 1994. Constant-pressure molecular-dynamics algorithms. *J. Chem. Phys.* 101:4177–4189.
22. Feller, S. E., Y. H. Zhang, …, B. R. Brooks. 1995. Constant pressure molecular dynamics simulation: the Langevin piston method. *J. Chem. Phys.* 103:4613–4621.
23. Essmann, U., L. Perera, …, L. G. Pedersen. 1995. A smooth particle mesh Ewald method. *J. Chem. Phys.* 103:8577–8593.
24. Miyamoto, S., and P. A. Kollman. 1992. Settle: an analytical version of the SHAKE and RATTLE algorithm for rigid water molecules. *J. Comput. Chem.* 13:952–962.
25. Bernèche, S., and B. Roux. 2003. A microscopic view of ion conduction through the K^+ channel. *Proc. Natl. Acad. Sci. USA.* 100:8644–8648.
26. Illingworth, C. J. R., S. Furini, and C. Domene. 2010. Computational studies on polarization effects and selectivity in K+ channels. *J. Chem. Theory Comput.* 6:3780–3792.
27. Furini, S., and C. Domene. 2013. K^+ and Na^+ conduction in selective and nonselective ion channels via molecular dynamics simulations. *Biophys. J.* 105:1737–1745.
28. Tang, L., T. M. Gamal El-Din, …, W. A. Catterall. 2014. Structural basis for Ca^{2+} selectivity of a voltage-gated calcium channel. *Nature.* 505:56–61.
29. Boiteux, C., I. Vorobyov, and T. W. Allen. 2014. Ion conduction and conformational flexibility of a bacterial voltage-gated sodium channel. *Proc. Natl. Acad. Sci. USA.* 111:3454–3459.
30. Jensen, M. O., V. Jogini, …, D. E. Shaw. 2013. Atomic-level simulation of current-voltage relationships in single-file ion channels. *J. Gen. Physiol.* 141:619–632.